UPPSALA
UNIVERSITET

UPTEC X 22021
Examensarbete 30 hp
Juni 2022

Modulation of a model ligand-gated ion channel by amphetamine derivatives

Emelia Karlsson

Civilingenjörsprogrammet i molekylär bioteknik

UPPSALA UNIVERSITET

Modulation of a model ligand-gated ion channel by amphetamine derivatives

Emelia Karlsson

Abstract

Pentameric ligand-gated ion channels are critical mediators of electrochemical signal transduction in neurons and other excitable cells, causing them to be important targets of psychoactive drugs. Structural data for these complex proteins are limited, particularly among eukaryotic family members and for the functionally critical open state. These data limitations cause knowledge gaps regarding the mechanisms of ion channel opening, gating, and modulation. However, a newly discovered bacterial family member, known as sTeLIC, shares numerous structural features with its eukaryotic relatives in our central nervous system. A recently solved electron microscopy structure depicts sTeLIC in an apparent open state with binding pockets in its extracellular domain, compatible with binding a drug with structural similarities to amphetamines, like the 4-bromoamphetamine. This project aims to provide the first structure-function evidence for direct modulation of a pentameric ligand-gated ion channel by an amphetamine.

The two most essential tools used in this project to examine the effects of 4-bromoamphetamine on sTeLIC were *Xenopus laevis* oocytes and two-electrode voltage-clamp. These tools were necessary for the collection of gating and modulation data. Ion channel activities can be analysed by clamping sTeLIC injected *Xenopus laevis* oocytes into the two-electrode voltage-clamp since it can artificially control the membrane voltage of oocytes.

Modulation data show that 4-bromoamphetamine is a bimodal allosteric potentiator, as well as an allosteric agonist. Residues Y104 and W75, located in the binding pocket, were selected by comparing the published open state model with an AlphaFold-generated non-conducting model. Mutating these into valine or alanine reduces the potentiation. One explanation may be that removing tyrosine's aromatic ring complicates retaining essential interactions in the binding pocket while swapping tryptophan for smaller residues could make it easier for the drug to stabilise the closed state.

Teknisk-naturvetenskapliga fakulteten

Uppsala universitet, Utgivningsort Uppsala

Handledare: Erik Lindahl & Rebecca J. Howard Ämnesgranskare: Annette Roos

Examinator: Johan Åqvist

sTeLIC - nyckeln som kan stoppa drogmissbruk?

Populärvetenskaplig sammanfattning

Emelia Karlsson

Vad är det som är osynligt för ögat men som påverkar hela ditt väsen? Jo, du gissade rätt...PROTEINER! Proteiner brukar kallas för kroppens byggstenar, vilket inte är konstigt då dessa små molekyler kan ha otaligt många olika funktioner. Vissa ger oss människor struktur och stadga, medan andra kan transportera ämnen till deras rätta destinationer i våra kroppar. Men vissa proteiner kan även sitta insprängda i våra cellmembran och därmed kallas för membranproteiner. Den här typen av proteiner är viktiga för oss tack vare att de fungerar som en kanal som kopplar samman cellernas inre med deras omgivning. Kanalerna har förmågan att öppna och stänga sig på ett sätt som tillåter olika molekyler att ta sig in och ut ur cellerna. De har dessutom en central roll i den intercellulära kommunikationen i våra nervsystem då de omvandlar kemiska signaler till elektriska impulser, exempelvis ansvarar de över vår motorik, tankar, tal och minne.

En grupp av membranproteiner som har visats vara lite extra viktiga för nervsystemet är de så kallade pentameriska ligandstyrda jonkanalerna, där namnet grundar sig på deras struktur. Men som det antydes tidigare så finns det en stor variation mellan olika proteiner. Skillnaden inom denna grupp av jonkanaler är att de binder och transporterar olika molekyler. Dessutom finns det studier som pekar på samband mellan icke-fungerande jonkanaler och drogmissbruk och neurologiska sjukdomar, exempelvis Alzheimers sjukdom och epilepsi.

Vår kunskap om pentameriska ligandstyrda jonkanalerna har ökat avsevärt de senaste åren men det finns mycket kvar att ta reda på. Nyligen upptäckte en forskargrupp i Frankrike en jonkanal från en bakterie som är väldigt lik våra egna jonkanaler, fast i en förenklad förpackning. Denna upptäckt kan öppna nya dörrar som kan hjälpa oss att förstå hur vi människor, rent mekaniskt, påverkas av droger. I det långa loppet skulle nya modeller göra det möjligt att reglera de ligandstyrda jonkanalerna för att hjälpa människor i drogmissbruk. I den här rapporten kommer ni få läsa om mitt examensarbete där jag kommer att vara med att tillhandahålla de första bevisen för struktur-funktion relationer av en pentamerisk ligandstyrd jonkanal, vid namn sTeLIC, med ett amfetaminderivat.

Examensarbete 30 hp
Civilingenjörsprogrammet i molekylär bioteknik
Uppsala universitet, juni 2022

Table of Contents

List of Abbreviations

4-BA 4-Bromoamphetamine

4-BrC 4-Bromocinnamate

cDNA Complementary DNA

CNS Central Nervous System

DMSO Dimethylsulfoxide

EC_{50} Half-Maximal Effective Concentration

ECD Extracellular Domain

ICD Intracellular Domain

pLGIC Pentameric Ligand-Gated Ion Channel

SEM Standard Error of Mean

TEVC Two-Electrode Voltage-Clamp

TMD Transmembrane Domain

WT Wild Type

1 Introduction

Pentameric ligand-gated ion channels (pLGICs) are critical mediators of electrochemical signal transduction in neurons and other excitable cells and are important targets of psychoactive drugs (Corringer *et al.* 2012, Plested 2016). Structural data for these complex proteins are limited, particularly among eukaryotic family members and for the functionally critical open state. Interestingly, several homologs of eukaryotic pLGICs exist in prokaryotes. These may be involved in diverse processes such as chemotaxis and pH sensing (Bocquet *et al.* 2009, Hilf & Dutzler 2008). Bacterial channels are often structurally and functionally simpler than eukaryotic subtypes. They often have truncated intracellular domains and are not as easily desensitised. Nonetheless, in some cases, they are sensitive to clinically important drugs, including alcohols (Howard *et al.* 2011, Sauguet *et al.* 2015), anaesthetics (Weng *et al.* 2010), and benzodiazepines (Spurny *et al.* 2012). Accordingly, bacterial pLGICs offer valuable model systems for structure-function studies of gating and modulation (Thompson *et al.* 2012).

One bacterial pLGIC, known as sTeLIC, was recently shown to be functionally accessible by heterologous expression in *Xenopus laevis* oocytes and activation at high pH (Hu *et al.* 2018). Further, an atomic-resolution structure of this channel was reported by X-ray crystallography to be in an apparent open state. Among other features, this channel contains pockets in its extracellular domain compatible with binding drugs (Hu *et al.* 2018), which are structurally similar to amphetamines. This class of psychostimulants has been shown to modulate eukaryotic pLGICs, but their sites and mechanisms of action remain unknown (Godden *et al.* 2001). In collaboration with researchers at the Pasteur Institute in Paris, we are in the process of collecting preliminary structural evidence to identify a binding site for an amphetamine derivative in sTeLIC. However, functional effects in this system have yet to be characterised.

This work will contribute in the short run to a structure-function understanding of sTeLIC modulation and mechanistic models of allosteric regulation in ligand-gated ion channels by drugs of abuse in the long run. Improving our mechanistic understanding of this family of neurotransmitter-gated ion channels has potential applications to the engineering-related pharmacological or therapeutic agents and in interpreting differential responses of eukaryotic channels to drugs.

1.1 Membrane Proteins

Proteins fulfil a wide range of functions in every kingdom of life. Proteins that are part of biological membranes fall into the category ”membrane proteins”; these members are further subdivided depending on their locations. Those that fully traverse the membrane are called transmembrane proteins, and such proteins interact with both the intracellular and extracellular environment of a cell, including the hydrophobic core of the phospholipid bilayer located in between (Figure 1) (Lodish *et al.* 2016, Almén *et al.* 2009).

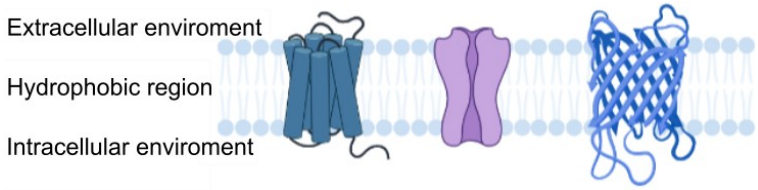

Figure 1. General illustrations of transmembrane proteins. Three generic membrane proteins fully traverse a phospholipid bilayer, linking the intracellular and extracellular environment of a cell, which may contribute to cellular communication. Created in BioRender.com.

Due to the broad spectrum of membrane proteins present in cells, these proteins can participate in various interactions and cellular processes, e.g. controlling concentration gradients between the intracellular and extracellular environments with the help of pumping mechanisms. Moreover, interactions between membrane proteins and molecules located in the extracellular surrounding may be contributing to enzymatic activity as well as cell-to-cell communication by converting chemical signals to electrical responses (Lodish *et al.* 2016, Nelson & Cox 2017).

1.1.1 Pentameric Ligand-Gated Ion Channels

The central nervous system (CNS) is one of our most critical organs since it controls most of our bodily functions, including movements, thoughts, speech, and memory (Callister & Graham 2010, Beyer *et al.* 1985, Turecek & Trussell 2001). Pentameric ligand-gated ion channels (pLGICs) belong to an important family of membrane proteins located in all three domains of cells; eukaryotes, prokaryotes and archaea. Even though the number of high-resolution structures of pLGICs have exploded in recent years, the majority of these structures are in non-conducting states (closed or desensitised) (Hilf & Dutzler 2008). pLGICs play an essential role in our CNS due to their ability to shift from a closed (resting) state to an open (active) state swiftly upon binding of agonists. Agonists can be anything from hormones and neurotransmitters to drugs, and when an agonist binds, a chemical signal is transduced, which induces conformational changes due to minor alterations in charge or protein folding, which alters the rate of gating transitions of the

pore. The opening allows ions to pass through, which creates an electrical signal that helps us execute our bodily functions (Kruse *et al.* 2013, Corringer *et al.* 2012).

It is this ability to mediate rapid synaptic communication that make pLGICs essential targets for the treatment of neurological disorders such as Alzheimer's disease (Rissman & Mobley 2011) and Parkinson's disease (Tanner *et al.* 2002). Prolonged exposure to agonists will make pLGICs transition into a long-lived desensitisation state, blocking them from activating even though agonists are present, and only when the agonist dissociates can the pLGICs return to their closed state. Furthermore, easily desensitised pLGICs are harder to capture in an open state because the transitioning between states is faster (Gielen & Corringer 2018).

Members of the pLGIC family consist of five identical subunits, each containing at least two of the following three domains: an extracellular domain (ECD), a transmembrane domain (TMD), and an intracellular domain (ICD) (Figure 2). ICDs are particularly prominent in eukaryotic pLGICs and have a role in receptor assembly, clustering, and trafficking (Thompson *et al.* 2010). ECDs have a β-sandwich immunoglobulin-like structure, and are a common binding area for agonists, while TMDs consist of four α-helices (M1-M4) that transverse the membrane. M2 is facing the channel pore, M1 and M3 create a second concentric circle around the M2 bundle, and M4 interacts with the membrane (Figure 2).

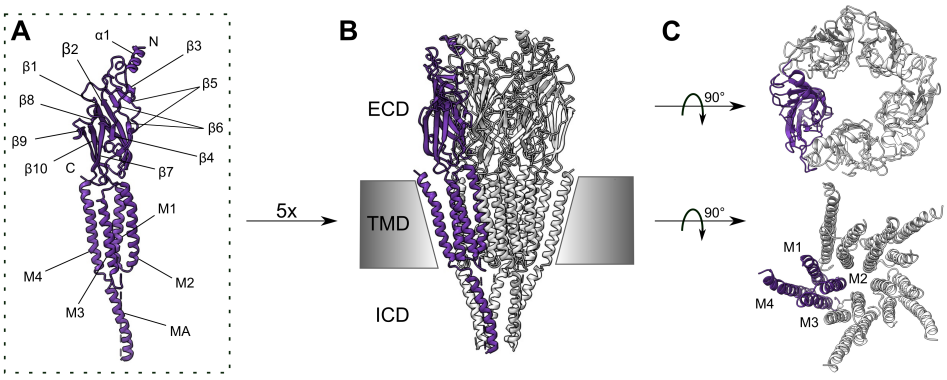

Figure 2. Generic structure representing pLGICs in a non-conducting state. A) Schematic representation of a single subunit. Secondary structure elements are highlighted: β-strands β1–β10, α-helix α1 are both located in ECD, M1–M4 in the TMD, and MA in the ICD. In addition, the C-terminal (C) and N-terminal (N) are presented. B) Side view perpendicular to the membrane (PDB ID: 2BG9 (Unwin 2005). For clarity, highlighting one subunit in purple. C) View from the extracellular side looking at solely the ECD and TMD. M1-M4 helices are labelled; M2 faces the pore channel while M4 interacts with the membrane.

1.1.1.1 Allosteric Modulation

The gating mechanism can be modulated by various psychoactive agents, e.g. alcohols, which may alter the amount of activation. It means that modulators can change the stability of the open state of an activated ion channel. Modulators are also ligands that bind somewhere on the receptor, but if these do not bind to the same site as an agonist, they are then so-called allosteric modulators. There are three types of allosteric modulators: positive, negative, and neutral. All may influence the level of activation of pLGICs by affecting the stability of their open state. They can affect the likelihood that an agonist binds or alter the agonist's effect on the pLGIC when binding (Figure 3). In addition, there are cases when modulators can activate channels by themselves; in such cases, these ligands are also classified as allosteric agonists (Neubig *et al.* 2003).

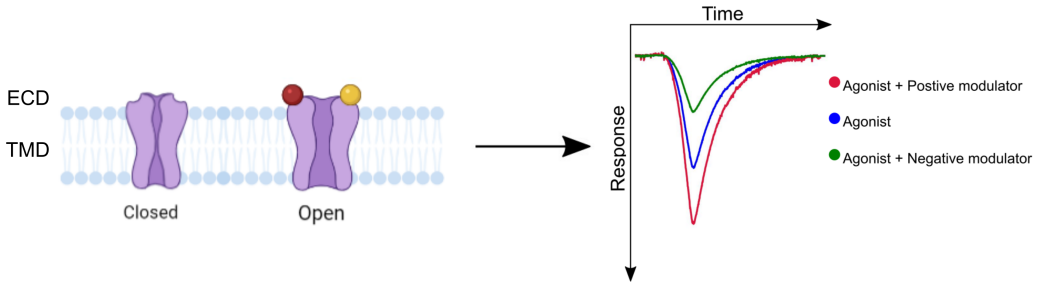

Figure 3. Schematic representation of an agonist and an allosteric modulator binding. The pLGICs are displayed in two possible states: a closed state and an open state. An agonist (red) and an allosteric modulator (yellow) have bound to the ECD in the open state. The allosteric modulator alters the stability of the activated channel, which influences the level of response and the number of ions that manage to pass through the channel before it goes back to its closed state. Created in BioRender.com.

1.1.2 sTeLIC

sTeLIC is a recently identified member of the pLGIC family that was structurally determined to be in a conducting (open) state (Hu *et al.* 2018). This gammaproteobacterial pLGIC has a wide opening around 11-15 Å, much broader than most members of its family. sTeLIC is a cationic channel that is activated at alkaline pH, meaning its agonist is the depletion of protons. On the other hand, divalent cations, e.g. Ca^{2+}, inhibit sTeLIC's gating transitions (Hu *et al.* 2018), this is a common trait for several other pLGICs (Zimmermann *et al.* 2012, Hilf *et al.* 2010). sTeLIC has a similar structure as its relatives, but Hu *et al.* (2018) has shown that sTeLIC has a specific cavity located in each ECD subunit that is a modulation site for 4-bromocinnamate (4-BrC) (Figure 4), which is structurally similar to amphetamine and its derivatives, e.g. 4-bromoamphetamine (4-BA).

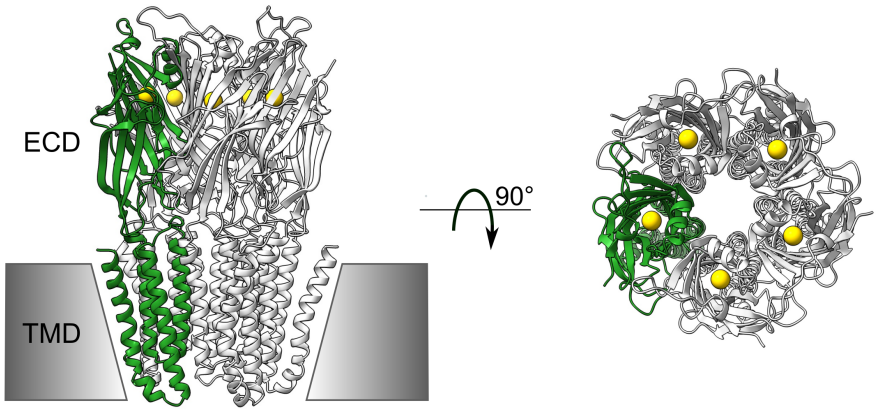

Figure 4. Overview of sTeLIC structure and the location of the modulatory sites. Cartoon representation of sTeLIC in an open state, along the axis perpendicular to the membrane (PDB ID: 6FL9). For clarity, one subunit is highlighted in green. Yellow spheres represent the location of the modulation site for 4-BrC, seen from the side and from the extracellular environment.

1.2 *Xenopus Laevis* Oocytes

Xenopus laevis is a type of African aquatic frog from the Pipidae family. Its oocytes have a conspicuous appearance, where they are divided into two distinct hemispheres, which are separated by a ”belt” (Figure 5). A darker animal pole-containing hemisphere and a lighter vegetal pole-containing hemisphere. This characteristic look is typical during the final stage (VI) of oocyte development (Dumont 1972), and the apparent separation between the poles is one factor that makes these oocytes an excellent model system for examining the expression of exogenous DNA/RNA and proteins in complex systems. Other factors that make oocytes great model systems are: easily obtained, low maintenance expenses (Mowry 2020), robust, and can remain in the final stage of oogenesis for years (Lin-Moshier & Marchant 2013). Background activity in oocytes is relatively low, which gives a high signal-to-noise ratio for membrane channel characterisation (Zampighi *et al.* 1995). But most importantly, *Xenopus* oocytes are capable of translating exogenous microinjected DNA/RNA due to their large size ($\sim$1.3 mm in diameter), so manual microinjection is possible. The microinjection procedure is also facilitated due to the distinct separation between the two hemispheres (Mowry 2020).

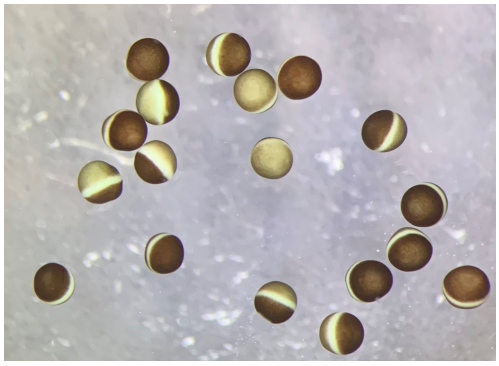

Figure 5. Snapshot of stage VI Xenopus oocytes taken under the stereomicroscope. Oocytes consist of two distinct hemispheres, an animal pole-containing hemisphere (dark brown) and a vegetal pole-containing hemisphere (light brown) separated by a "belt" (creamy white).

1.3 Two-Electrode Voltage-Clamp Electrophysiology

Two-electrode voltage-clamp (TEVC) is an electrophysiological technique that allows the user to analyse ion channel activities by artificially manipulating the membrane voltage of the oocytes. TEVC is especially important in the biophysical field since it can increase our understanding of the fundamental biophysical properties of ion channels. Specifically, TEVC combined with *Xenopus* oocytes can study the exogenous expression of ion channels (Guan *et al.* 2013).

A schematic illustration of a general setup for TEVC recording of an oocyte is depicted in Figure 6. A voltage electrode (E_V), connected to a voltage monitoring amplifier (A_1), measures membrane potentials (V_m). Since A_1 has a high impedance, a small electrical current is drawn from the oocyte. The output of A_1 is attached to a negative feedback amplifier (A_2). A_2 can compare V_m with the voltage command (V_c), also fixated to the input of A_2. The value of V_c is set manually via the computer at the desired membrane voltage. To clarify, A_2 has V_m and V_c as inputs; the resulting output will be an electrical current proportional to the input difference; forced into the oocyte via a current electrode (E_I). In other words, A_2 will calculate the difference between V_m and V_c as an "error" and compensate for this offset, causing E_I to inject electrical current into the system (Guan *et al.* 2013). Two bath electrodes are also attached to the system via agarose bridges. One of them will act as a reference for E_V, and the other one works for grounding and determining the electrical current flow over the membrane that E_I injects (Halliwell *et al.* 1994).

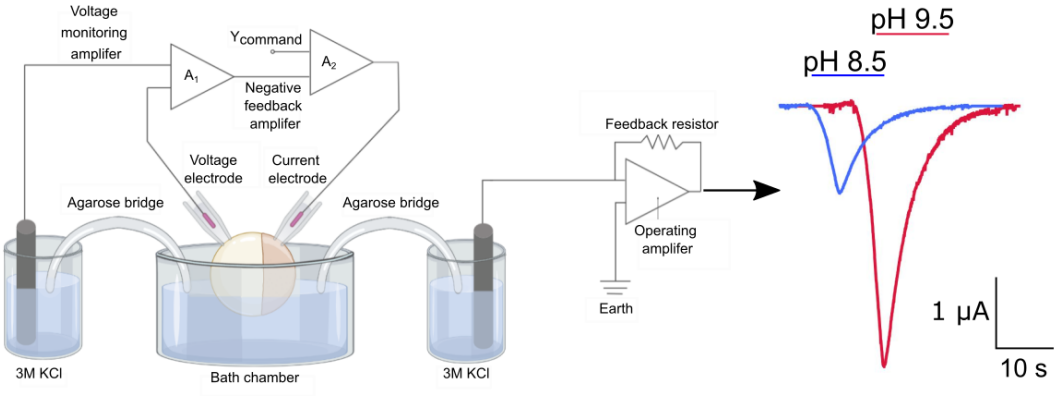

Figure 6. Schematic illustration of TEVC applied to a Xenopus oocyte (left) and an example of typical current traces (right). For a detailed description, see the text above. The blue and red lines above the current traces represent the duration of the applied buffer at different pHs. Adapted from (TEV 2018) and created in BioRender.com.

1.4 Aims

This project aims to provide the first structure-function evidence for direct modulation of a pLGIC by an amphetamine. Quantifying the effects of 4-bromoamphetamine on sTeLIC function will be done with TEVC-electrophysiology in *Xenopus* oocytes. Subsequent steps will involve molecular visualisation of preliminary structural data, and the design and characterisation of mutants predicted to alter amphetamine binding or modulation.

2 Materials and Methods

All buffers and analytical grade reagents, prepared with Milli-Q water, were stored at 4° C. 4-BA purchased from National Measurement Institute (Canberra, Australia) was dissolved in dimethylsulfoxide (DMSO) and kept at 4° C as a 1M stock solution.

2.1 Equipment

Equipment stated below was required to carry out cDNA injections and TEVC recordings described in sections 2.3 and 2.4. For reference, the equipment used is stated in parentheses with its distributors.

- Microinjector (Nanoject II Auto-Nanoliter Injector, Drummond Scientific, Broomall, PA)
- TEVC amplifier (OC-725C amplifier, Warner Instruments, Hamden, CT)
- Digitizer (Digidata 1440A, Molecular Devices, Sunnyvale, CA)
- TEVC software (Clampex, Molecular Devices, Sunnyvale, CA)
- Stereomicroscope (SMZ1000, Nikon, Natori, Japan)
- Perfusion system (Custom-made)
- Micropipette puller (PC-10 Puller, Narishige International, Tokyo, Japan)
- Glass capillaries (e.g. Drummond #3-000-203-G/XL and Harvard #30-0053)

2.2 Maintenance of Oocytes

All *Xenopus* oocytes were purchased from EcoCyte Bioscience (Dortmund, Germany) and those that looked deformed or lacked a clear separation between the two hemispheres, were discarded. Stage V and VI oocytes were stored in modified Barth´s solution (88 mM NaCl, 1 mM KCl, 2.4 mM $NaHCO_3$, 0.91 mM $CaCl_2$, 0.82 mM $MgSO_4$, 0.33 mM $Ca(NO_3)_2$, 10 mM HEPES, 0.5 mM theophylline, 0.1 mM G418, 17 mM streptomycin, 10,000 U/l penicillin and 2 mM sodium pyruvate, that was passed through a 0.22 μm filter and adjusted to pH 7.5) at 13° C in an incubation chamber.

2.3 cDNA Injection

Glass capillaries with ∼20 µm tips, pulled with a PC-10 Narishige Puller, were filled with mineral oil and installed onto the Nanoject II. A ∼2 µL drop of sTeLIC cDNA was positioned onto a piece of parafilm under the stereomicroscope. cDNA was loaded into the glass needle by negative pressure before an oocyte channel was placed under the stereomicroscope (Figure 7).

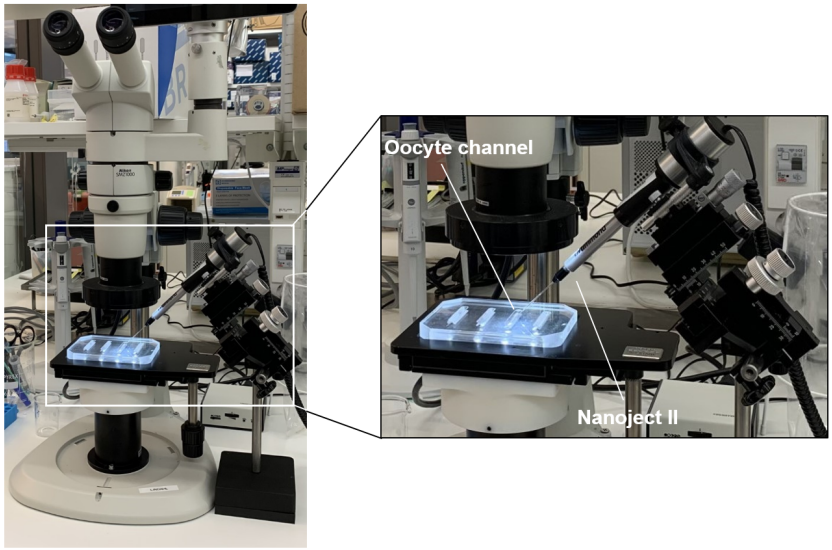

Figure 7. Injection setup. A Nanoject II is standing on the stereomicroscope's right-hand side. An oocytes channel is placed under the stereomicroscope.

A couple of oocytes were transferred onto the oocyte channel with a glass pipette. Oocytes were injected (6 ng/32.2 µl) into their darker hemisphere, since the animal pole is located there, before being relocated into a 48-well plate containing modified Barth´s solution. Plates containing oocytes were stored at 13° C in the incubation chamber for 5-10 days before TEVC experiments occurred.

2.4 Oocyte Electrophysiological Recording

A voltage electrode and a current electrode containing chloride-plated silver wires were incorporated onto glass electrodes containing 3 M KCl. Oocytes were perfused in pH 7.5 Ringer's buffer with Ca^{2+} at a rate of 20 rpm in a bath chamber. Ringer's buffer contained: 123 mM NaCl, 2 mM KCl, 2 mM $MgSO_4$ and 2 mM $CaCl_2$. An oocyte bath clamp and two agar bridges were installed into the ground stages filled with 3 M KCl. The bridges connect the ground stages with the bath chamber and the waste chamber. The voltage electrode and the current electrode were positioned onto the electrode holders (Figure 8). An oocyte was relocated into the bath chamber, with the electrodes slightly touching its membrane. The clamping was set to -40 mV using an OC-725C amplifier, Digidata 1440A, and the software Clampex.

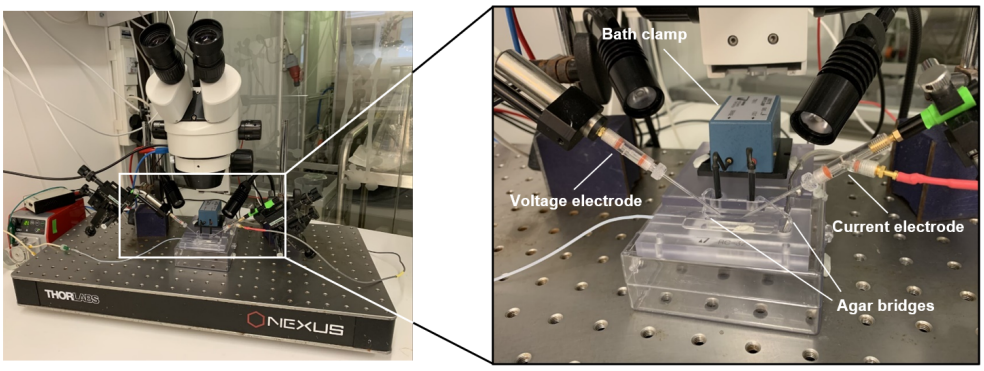

Figure 8. TEVC setup. Overview showing microscope and the TEVC platform (left). For clarity, essential components of the equipment are pointed out (right).

In order to avoid inhibition of the sTeLIC due to Ca^{2+}, buffers were prepared without it. Therefore the Ca^{2+}-containing pH 7.5 buffer was exchanged for a Ca^{2+}-free variant. Depending on the expression level of sTeLIC channels, the electrical current will drop and stabilise, creating a new baseline. When the baseline was established, the Ca^{2+}-free pH 7.5 buffer was changed to Ca^{2+}-free pH buffer between pH 8-10 for 30 s before being switched back to the Ca^{2+}-free pH 7.5 buffer for 12 min. Then a new Ca^{2+}-free alkaline buffer (pH 8-10) was applied. When no further applications were required, the buffer was changed to the Ca^{2+}-containing pH 7.5 to deactivate sTeLIC.

The same procedure was used when the modulatory effects of 4-BA were tested. The wash periods with Ca^{2+}-free pH 7.5 buffer were 5 min, and application times were still 30 s. Instead of applying buffers with different pH, only pH 8.5 buffers were applied. Some contained different concentrations of 4-BA (6 μM, 20 μM, 60 μM and 200 μM)

and one without. After a drug-containing pH 8.5 buffer application, the two upcoming applications were drug-free to ensure complete re-sensitisation of the ion channels.

To investigate whether 4-BA could activate sTeLIC by itself, the oocytes were washed for 5 min in Ca^{2+}-free pH 7.5 running buffer to obtain a new baseline with activated sTeLIC. The buffer was changed to one with the same conditions, except it contained 4-BA for 1 min. This buffer was immediately switched to a drug-containing pH 8.5 buffer with the same concentration for 30 s.

2.5 Statistics

All statistical analyses of electrophysiology data were performed with Prism 9.3.1 (GraphPad Software, La Jolla, CA). Fitting of activation curves with non-linear regression, using the following equation:

$$Y = R_{basal} + \frac{R_{max} - R_{basal}}{1 + 10^{[log(EC_{50}) - X]}} * n_H \tag{1}$$

, where Y is the activation response, R_{max} is the maximal response, R_{basal} is the baseline, X is the proton concentration, EC_{50} is the concentration of a drug that induces 50 % of maximal response, and n_H is the Hill coefficient. The EC_{50} could be extracted from the sigmoidal-shaped activation curve. The EC_{50} is used to compare how easily ion channel variants are activated, e.g. a lower value leads to a left shift which means the activation occurs at lower pH. All pH activation data (pH 8-10) are calculated as:

$$\textit{relative current} = \frac{R_A}{< R_0, R_1 >} \tag{2}$$

, where R_A represents activation responses, and $<R_0,R_1>$ portrays the mean of responses occurring right before and after the R_A response. These data points are then calculated as mean $\pm$ SEM and are fitted to the Hill model (Equation 1).The same goes for calculating %modulation:

$$\%modulation = \frac{R_A - < R_0, R_1 >}{< R_0, R_1 >} * 100 \tag{3}$$

, but the mean $\pm$ SEM data is not fitted to the Hill model and are instead depicted in column graphs.

2.6 Mutagenesis

For mutagenesis, UCSF Chimera 1.15 (Pettersen *et al.* 2004) was used to visualise how 4-BA might bind around the binding site that is a confirmed binding pocket for the structurally similar molecule, 4-BrC. Residues of interest were selected by comparing the binding pocket of the published open state structure (Hu *et al.* 2018) with an AlphaFold generated non-conducting state model. Commercially made mutagenic primers (Invitrogen, Stockholm, Sweden) and a cycle sequencing method (Eurofins Genomics GmbH, Ebersberg, Germany) was used to confirm the mutations. cDNAs were prepared using HiSpeed® Plasmid Midi Kit (Qiagen GmbH, Hilden, Germany).

3 Results

3.1 Conditions for sTeLIC Activation

Electrophysiology data show that sTeLIC is open at basic pHs, and the activation increases with pH. Further, the removal of Ca^{2+} creates a baseline shift which suggests that sTeLIC gets inhibited by divalent cations and thus is consistent with results published by Hu *et al.* (2018). Since the absence of Ca^{2+} activates sTeLIC, it was possible to detect changes in electrical current when exchanging the pH 7.5 recording buffer to high pH Ca^{2+}-free buffer. The smallest increases in activation responses occurred at pH 8 and maximal at pH 10 (Figure 9A). Fitting the pH activation data to the Hill model (Equation 1) yielded an $\log EC_{50}$ of 8.9 (Figure 9B). pH activation data are usually normalised to maximal pH to reduce potential noise. The two highest pH buffers initially contained CAPS (buffering agent) and had to be remeasured because this agent created an extra artificial response. To avoid remeasuring all activation data, the next pH buffer inline (pH 9) had to be the reference.

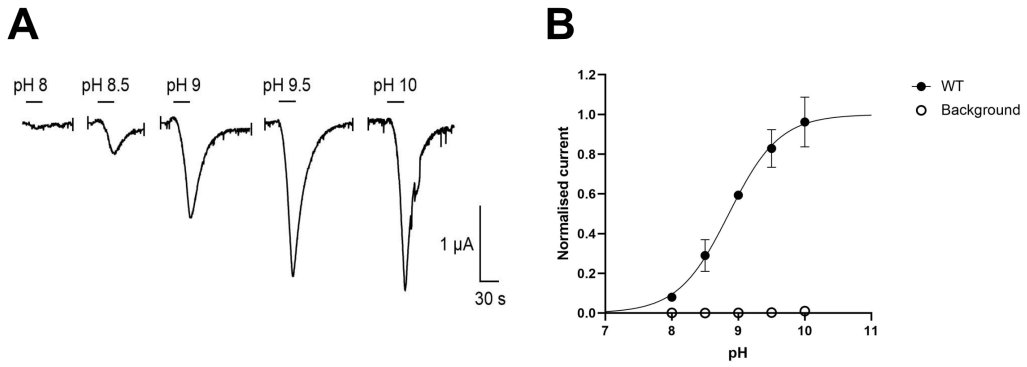

Figure 9. sTeLIC activation at alkaline pH. A) Representative current trace of sTeLIC. Application time for Ca^{2+}-free alkaline buffers was 30 s. Larger sections of the 12 min long wash periods of the Ca^{2+}-free pH 7.5 buffer have been excluded. Bold lines represent when the alkaline buffer was added. B) Two response curves are displayed in black and white, representing the mean peak height for the increased activation at each pH depicted in (A) ($n \geq 4$). Black circles represent mean peak activation data from sTeLIC expressing oocytes. Meanwhile, white circles represent background noise from non-injected oocytes. All data points are normalised to activation data at pH 9. In addition, white circles are normalised to pH 9 data from injected oocytes.

3.2 Identification of 4-BA as an Allosteric Modulator

Significant potentiation was observed when applying 4-BA to sTeLIC WT (Figure 10A). The column graph depicts a dose-dependent degree of modulation (Figure 10B), where the lowest level of potentiation occurred at 6 µM 4-BA and the highest at 60 µM. The activation potentiation by $\sim$ 60 % and by $\sim$ 280 %, respectively. The potentiation steadily increased from 6 µM to 60 µM, whereas at 200 µM, the level was similar to 6 µM, namely $\sim$ 66 %.

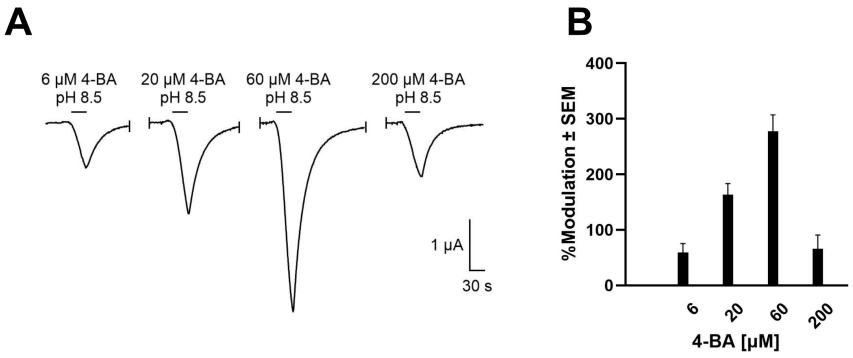

Figure 10. Dose-response data on sTeLIC WT with 4-BA. A) Representative current trace from sTeLIC shows how drug-containing Ca^{2+}-free pH 8.5 buffers greatly enhanced the activation response up to 60 µM 4-BA and decreased at 200 µM. Two drug-free applications in pH 8.5 buffer between each drug-containing application are excluded. Bold lines represent when the drug-containing buffer was added. B) Represent the level of mean modulation in % with indicated SEM for specific 4-BA concentrations ($n \geq 4$).

3.3 Activation in Neutral pH

Activation occurred when the Ca^{2+}-free pH 7.5 running buffer contained 60 µM or 200 µM 4-BA (Figure 11A). The activation increased with $\sim$ 20 % in pH 7.5 with 60 µM 4-BA, whereas the increasing was $\sim$ 90 % with 200 µM 4-BA (Figure 11B).

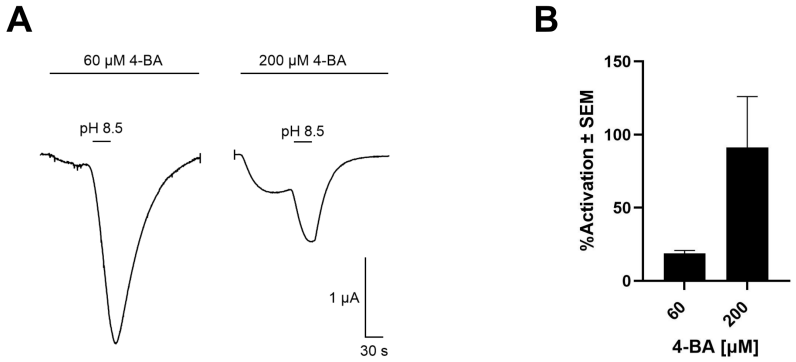

Figure 11. sTeLIC activation at pH 7.5 with 4-BA. A) Current traces show how the activation of sTeLIC increases with a higher concentration of 4-BA in pH 7.5. Two drug-free applications in pH 8.5 buffer between each drug-containing application are excluded. Bold lines illustrated when the drug-containing buffer was added. B) The level of increased mean activation in % with indicated SEM for 60 µM and 200 µM 4-BA ($n \geq 3$).

3.4 AlphaFold Generated Non-Conducting Models

Due to Hu *et al.* (2018), I have a structure of sTeLIC in an apparent open state, but an experimentally determined closed state is still missing. However, AlphaFold 2 generated five non-conducting states of sTeLIC. The highest-ranked prediction is depicted with other relatives in experimentally determined non-conducting states. The pore profile shows similarities between the AlphaFold-generated sTeLIC model and three published relatives, DeCLIC, ELIC and GLIC, all in non-conducting states (Figure 12).

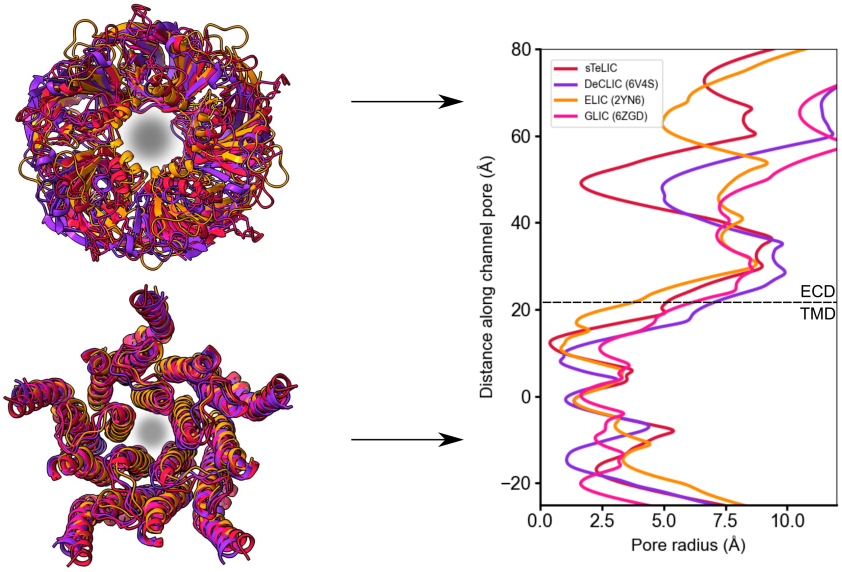

Figure 12. Non-conducting state comparison between sTeLIC (red), DeCLIC (PDB ID: 6V4S (purple)), ELIC (PDB ID: 2NY6 (orange)) and GLIC (PDB ID: 6ZGD (pink)). Superimposed ECDs and TMDs, both seen from the extracellular side. Arrows point to which half of the pore profile graph each structure represents. The size of the grey circle is compared throughout the whole pore channel for both compartments.

3.5 ECD Contraction Upon Pore Opening

To get an idea of how 4-BA may bind to sTeLIC and what the outcome of such interaction could be, I had to compare the published open state with the non-conducting AlphaFold model. Two changes within the two domains were observed, namely, upon pore opening of the ECD contracts. The most significant difference occurs in the TMD, the non-conducting model more or less closing the pore (Figure 13).

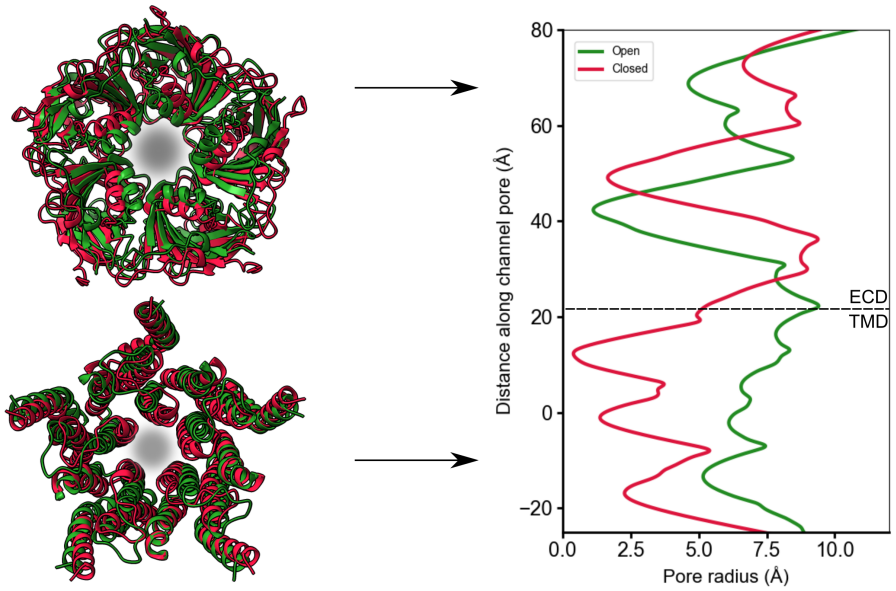

Figure 13. State comparison. The published open state model (green) and the AlphaFold-generated non-conducting state model (red) are superimposed to compare pore radius. Arrows point to which half of the pore profile graph each structure represents. The size of the grey circle is compared throughout the whole pore channel for both compartments. The ECD radius in the open state is smaller than in the non-conducting model. The M2 helices in the non-conducting model are closer to each other.

3.6 4-BA Binds to the Open State

To gain structural information on how 4-BA binds to the modulation site, I had to look closer at the residues at this site and locate differences between the two states. The binding pocket is located in the middle of the ECD, whose entrance is located on the inside of the pore at the β-sandwich immunoglobulin-like structure (Figure 14B). Multiple local docking simulations were done by AutoDock Vina (Trott & Olson 2010) in Chimera. This program uses an empirical scoring function to estimate the affinity of protein-ligand binding, and a negative score implies that the binding is favourable, while a positive score implies an unfavourable binding. The docking simulations showed that 4-BA achieves a favourable binding when it positions itself parallel with Y104 and when W75 has flipped away from the pocket (Figure 14C). The ligands in the open state scored binding energies between -4.8 < kcal/mol < -3.9 and between 13.4 < kcal/mol < 13.9 for the non-conducting state.

W75 acquires two completely different rotamers in the two states (Figure 14C and 14D) and as shown in Figure 13, the ECD subunits in the open state are positioned closer to each other; allowing interactions between subunits (Figure 14E). W75 interacts with one residue on the neighbouring β5 and two on β3. These three residues are the following; L93, T58, and T60. All three residues are within 4 Å. The loop containing W75 in the non-conducting state is shifted an additional $\sim$ 4 Å away from its neighbouring subunit compared to the open state.

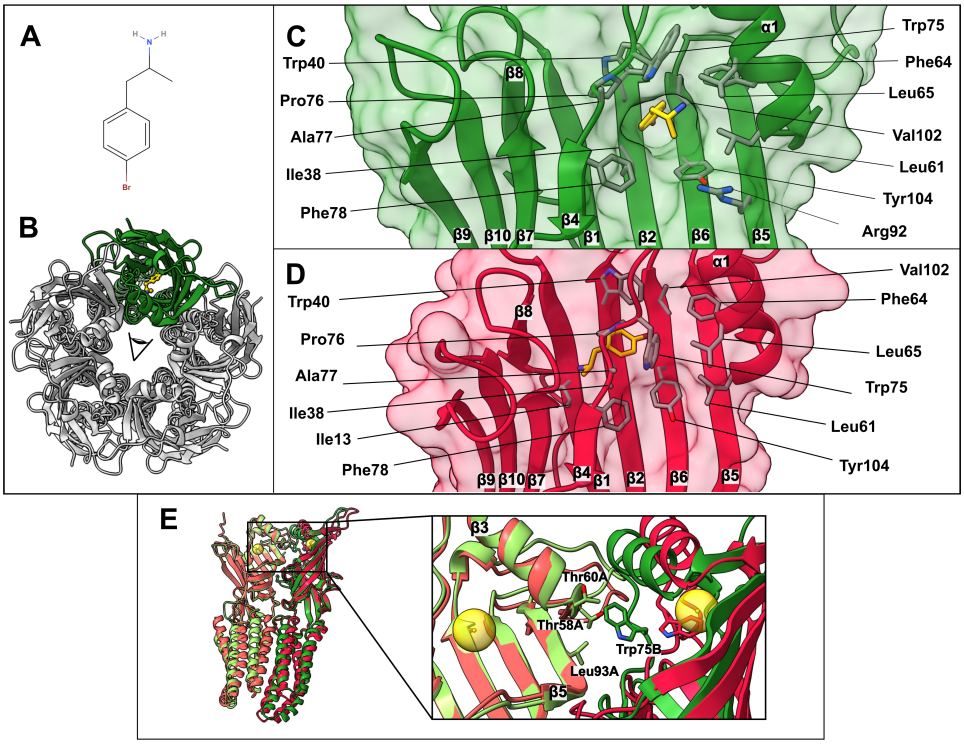

Figure 14. Docking site comparison. A) The structural formula of 4-BA. B) Simulated docking position of 4-BA (yellow) in the open model´s ECD (green), seen from the extracellular side. 4-BA shown in stick and ball style. C, D) Close-up view of the interaction between 4-BA and sTeLIC in the (C) open state (green) and (D) non-conducting state (red) in cartoon and surface representation. Residues within 4 Å are depicted as sticks and labelled. E) W75 in the open state (green) acquires multiple bonding interactions with residues located in the neighbouring subunit (light green). Displayed residues are within 4 Å of W75, namely L93 located on β5 and T58 and T60 on β3. Yellow spheres represent an approximated location of the modulation site for 4-BA.

3.7 F16' Closes the Pore

What we already know from Hu *et al.* (2018) is that the diameter of the pore in the open state is around 11-15 Å (Figure 15A and 15C). Residues on the M2 helices that faced into the pore were; D-4', D2', G6', L9', I12', A13', F16', T17', and S20' (Figure15C). The most significant changes are residues, F16', L9' and K-1'. All are facing into the pore in the non-conducting state, closing the pore. The restricted regions have diameters of 0.6 Å, 3.7 Å, and 4.2 Å, respectively (Figure 15B and 15D).

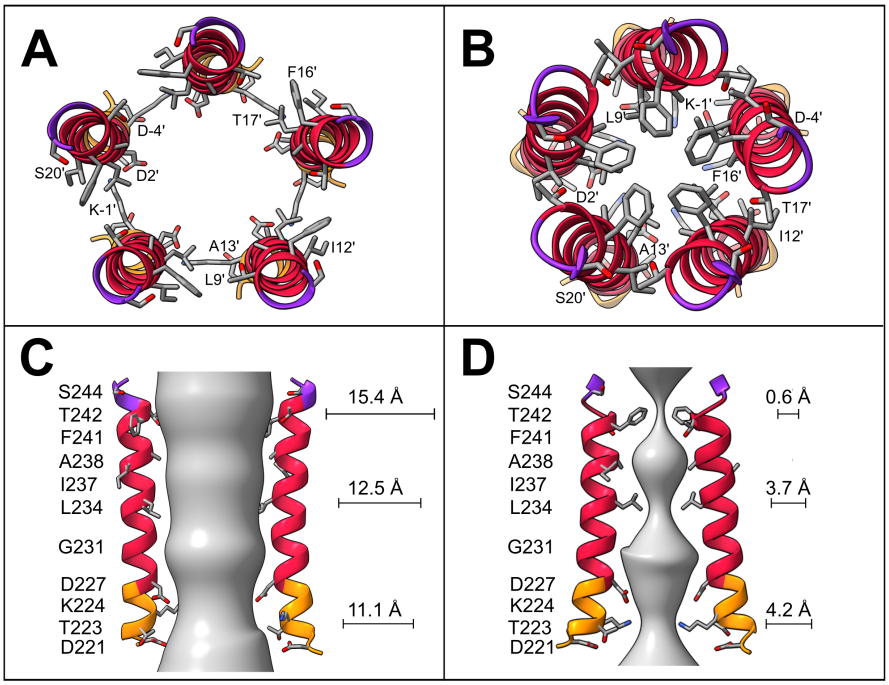

Figure 15. Pore comparison. Overall properties of the residues are coloured as follows; purple (polar), red (hydrophobic), and orange (charged). A, B) M2 α-helices seen from the extracellular side for the (A) open state and (B) non-conducting state. The stick format illustrates residues facing the pore. C, D) Side view of M2 α-helices with a pore coloured in grey in between. Residue numbering (left) and pore diameter (right) for F241, L234 and K224 are displayed.

3.8 Potentiation Reduced Among Mutants

Two residues that were distinct from the rest in the binding pocket were Y104 and W75 (Figure 16A). I generated and examined four mutants; Y104A, Y104V, W75A, and W75V. In the same order, extracted logEC_{50} from the activation curves (Figure 16B) for

the mutants were 9.4, 8.7, 10.2, and 8.7. All mutants responded less to 4-BA compared to WT, hardly any potentiation occurred at 6 μM and less than 100-fold potentiation is seen for 20 μM and 60 μM. At a concentration of 200 μM, both W75 potentiated more than the WT (Figure 16C), and especially W75V, which potentiated twice as much as WT.

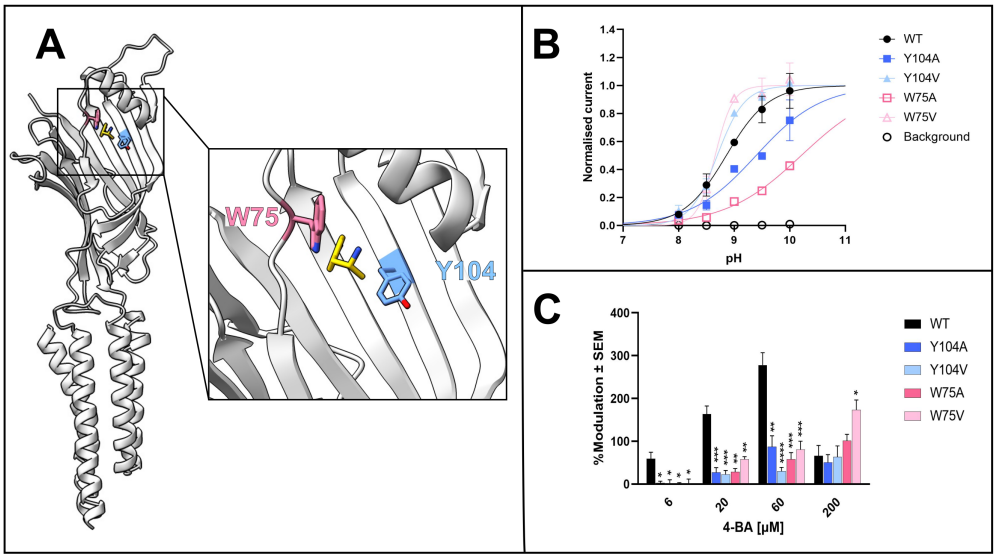

*Figure 16. Mutant modulation. A) Overview of a subunit showing location of Y104 (blue) and W75 (pink) with respect to 4-BA (yellow). B) Response curves for WT and four mutants. Mutants of W75 are coloured in shades of pink meanwhile Y104 mutants are in blue. In addition, alanine mutants are represented in squares and valine as triangles. Normalised with respect to activation data at pH 9 and mean activation data spans from pH 8-10 with 0.5 increments. C) Average potentiation of mutants compared with WT at multiple concentrations of 4-BA ($n \geq 3$). The significance is relative to WT (*P < 0.01, **P < 0.001, ***P < 0.0001, ****P < 0.00001).*

4 Discussion

The aim of this project was to provide the first structure-function evidence for direct modulation of a pLGIC by an amphetamine. Based on my experiments, I drew the hypothesis that 4-BA is a bimodal allosteric potentiator and an allosteric agonist at high concentrations. Mutating Y104 and W75 into smaller hydrophobic residues reduces the potentiating effects of sTeLIC. The upcoming sections are elaborations on my hypothesis.

4.1 Allosteric Potentiation of sTeLIC via 4-BA

There is no doubt that preliminary data suggest that 4-BA is a potentiator since the potentiation increased markedly from 6 μM to 60 μM with a 100-fold for each measuring point (Figure 10B). At even higher concentrations, the potentiation is reduced to roughly the same levels as in applications with 6 μM. This indicates that 4-BA has bimodal effects, otherwise, we would have seen a sigmoidal-shaped trend curve over the column graph. This means that it can potentiate and inhibit pLGICs activation. Inhibition at higher concentrations is characteristic, which has been seen among multiple relatives (Howard *et al.* 2011, Fourati *et al.* 2018). Possible explanations for this reduction at 200 μM could be that it has been more desensitised or that higher concentrations of 4-BA increase the probability of binding low affinity inhibitory binding sites, which has been seen among other relatives. It could also have something to do with solubility and aggregation, but this is probably not the case since we can see direct activation that increases with higher concentrations (Figure 11).

The local docking simulations prove that 4-BA binds to the open state (Figure 14). Since the scoring is based on binding energies, a negative score means favourable binding. A distinct difference in scoring was shown; the non-conducting state had scores above 13 kcal/mol while the open scored -4.8 < kcal/mol < -3.9.

4.2 Reduced Modulatory Effect by Mutants

For Y104A and Y104V in Figure 16C, we can see decreased effects of 4-BA. My initial hypothesis was that Y104 has a stabilising impact due to the aromatic ring in 4-BA being parallel to Y104, which could create stable pi-stacking interactions that can retain it in the binding pocket. The removal probably reduces 4-BA's total avidity since the ligand cannot be positioned in a necessary way that can maintain essential interactions to stabilise the open state. However, the trend is not that clear, and therefore I can only say for certain that removing the aromatic ring has a role in the stabilisation of the open state.

A reduction in potentiation is also seen among the W75 mutants. My preliminary hypothesis was that this residue would act as a door that allows ligands to enter the binding pocket. Therefore, there should be room for 4-BA to enter, especially in the alanine case, and thus the modulation would increase. This cannot be the case, but it could be the other way around; namely, W75 makes sure that 4-BA does not leave the binding pocket too quickly. This means that the bigger the residue, the harder it is for the ligand

to slip out, and therefore, W75V has a more potent potentiation compared to W75A. Even though the trend is more explicit here, this is just speculation. It could also be that the removal of W75 exposes the binding pocket, allowing 4-BA to stabilise the closed state. However, as shown in Figure 14E, the W75 interacts with residues from another subunit. Perhaps W75 acts in the transition between open and closed form. So even though ligands get into the binding pocket, the pore cannot open, since both alanine and valine are not long enough to create essential interactions to switch completely between states.

4.3 Reliability of AlphaFold Models

Due to Hu *et al.* (2018), I have a structure of sTeLIC in an apparent open state, but an experimentally determined closed state is still missing. Therefore, I considered using AlphaFold 2 since it uses artificial intelligence to build predictions by comparing a protein sequence to a database of sequences with solved structures in hope of getting a model in a closed state. But I had an open mind because I did not know what I would come across in the end. Since my ”closed” model is generated via AlphaFold 2 and not experimentally determined, it is difficult to say how biased the model is due to being influenced by published closed state models. In order to find valuable residues to mutate, having the closed model has been an advantage because it shows potential differences that may be interesting to investigate. I believe that I would not have looked further into W75 if a closed state model was not available, and I would have missed facts that suggest that W75 has a significant role as a ”door” to the binding site of the modulator (Figure 14). In addition, I would also have overlooked the ”flipping” of W75 that can be involved with subunit interactions. As well as that, the loop connecting β4 and α1 can be shifted closer to the neighbouring subunit and thus allows residues in the vicinity to interact and ”hold up” W75 from the binding (Figure 14E).

The model also feels believable due to the look of the pore channel. The TMD region holds eye-catching dissimilarities at F241, L234, and K224. These residues, and especially F241, shut the passage through the membrane when the pore diameter here is less than 1 Å, namely 0.6 Å (Figure 15D), which differs from the open state since the pore diameter is around 11-15Å throughout the TMD, as the majority of residues point away from the pore. But in the end, the only thing that can determine the reliability of the AlphaFold model is that experiments produce a closed-form.

4.4 Future Prospects

Although the AIs of today for determining protein structures are exceptional and can give us an idea of where to start looking when investigating structure-function relationships, only an experimentally determined model can provide a complete understanding of the function and characteristics. Therefore, future work involves determining a closed state experimentally and an open one with 4-BA in the binding pocket, but also to see if there are more binding sites where 4-BA binds. It would be fascinating to see how realistic the AlphaFold model is. These models can be used to see how conserved this response is among human channels and look for equivalent binding sites, which can not be seen in the sequence alignment.

More research is required to be able to conclude the exact reasons why the level of potentiation was reduced for the mutants. In addition, the mutants can be investigated to see if they can also activate the ion channel directly.

5 Conclusion

In conclusion, the analysis above supports that 4-BA works as a bimodal allosteric potentiator that can also activate pLGICs by itself. In addition, structure comparison proves that 4-BA binds only to the open state, which means the interaction is state-dependent. Lastly, all four engineered mutations validate an ECD binding site for amphetamines.

6 Acknowledgement

First of all, I want to show my appreciation to my supervisors Erik Lindahl and Reba Howard for giving me this opportunity to carry out my Master's thesis in the Molecular Biophysics Stockholm group at SciLifeLab, Solna. During these few months I have been here, my knowledge of this important area, that I had barely come into contact with before, has grown ridiculously big. I have never been so fascinated by a particular field before. One key person that I want to show extra gratitude to is you, Reba. Your enthusiasm in combination with your astounding knowledge and experience have offered me

invaluable guidance, support, and motivation throughout this project. I believe that you have helped me grow as a person and as a scientist.

Special thanks are extended to Urška Rovšnik, Marie Lycksell, Olivia Andén, and Farzaneh Jalalypour for helping me in the lab and with computational difficulties. But I also want to acknowledge the rest of my colleagues at Molecular Biophysics Stockholm for being so helpful and supportive all my weeks. All of you have shared your knowledge and time, and I am very grateful.

I want to take the opportunity to express my gratitude to Annette Roos, Researcher at the Department of Cell and Molecular Biology at Uppsala University for being my scientific reviewer. I would also like to thank my examiner Johan Åqvist, my course coordinator Lena Henriksson as well as my opponent Johanna Cederblad for your help and feedback during the project.

References

2018. TEVC setup. WWW-document: https://www.deviantart.com/rieile/art/TEVC-setup-734868338. Retrieved 2022-01-24.

Almén MS, Nordström KJ, Fredriksson R, Schiöth HB. 2009. Mapping the human membrane proteome: a majority of the human membrane proteins can be classified according to function and evolutionary origin. BMC Biology 7: 1–14.

Beyer C, Roberts LA, Komisaruk BR. 1985. Hyperalgesia induced by altered glycinergic activity at the spinal cord. Life sciences 37: 875–882. Elsevier.

Bocquet N, Nury H, Baaden M, Le Poupon C, Changeux JP, Delarue M, Corringer PJ. 2009. X-ray structure of a pentameric ligand-gated ion channel in an apparently open conformation. Nature 457: 111–114. Nature Publishing Group.

Callister RJ, Graham BA. 2010. Early history of glycine receptor biology in mammalian spinal cord circuits. Frontiers in molecular neuroscience 3: 13. Frontiers.

Corringer PJ, Poitevin F, Prevost MS, Sauguet L, Delarue M, Changeux JP. 2012. Structure and pharmacology of pentameric receptor channels: From bacteria to brain. Structure 20: 941–956. Elsevier.

Dumont JN. 1972. Oogenesis in *Xenopus laevis* (daudin). i. stages of oocyte develop-

ment in laboratory maintained animals. Journal of morphology 136: 153–179. Wiley Online Library.

Fourati Z, Howard RJ, Heusser SA, Hu H, Ruza RR, Sauguet L, Lindahl E, Delarue M. 2018. Structural basis for a bimodal allosteric mechanism of general anesthetic modulation in pentameric ligand-gated ion channels. Cell reports 23: 993–1004. Elsevier.

Gielen M, Corringer PJ. 2018. The dual-gate model for pentameric ligand-gated ion channels activation and desensitization. The Journal of Physiology 596: 1873–1902. Wiley Online Library.

Godden EL, Harris RA, Dunwiddie TV. 2001. Correlation between Molecular Volume and Effects of *n*-Alcohols on Human Neuronal Nicotinic Acetylcholine Receptors Expressed in *Xenopus* Oocytes. Journal of Pharmacology and Experimental Therapeutics 296: 716–722. ASPET.

Guan B, Chen X, Zhang H. 2013. Two-electrode voltage clamp. Ion Channels, Springer, 79–89.

Halliwell JV, Plant TD, Robbins J, Standen NB. 1994. Voltage clamp techniques. Microelectrode Techniques. The Plymouth Workshop Handbook. The Company of Biologists, Ltd. Cambridge, 17–35.

Hilf RJ, Bertozzi C, Zimmermann I, Reiter A, Trauner D, Dutzler R. 2010. Structural basis of open channel block in a prokaryotic pentameric ligand-gated ion channel. Nature structural & molecular biology 17: 1330–1336. Nature Publishing Group.

Hilf RJ, Dutzler R. 2008. X-ray structure of a prokaryotic pentameric ligand-gated ion channel. Nature 452: 375–379. Nature Publishing Group.

Howard RJ, Murail S, Ondricek KE, Corringer PJ, Lindahl E, Trudell JR, Harris RA. 2011. Structural basis for alcohol modulation of a pentameric ligand-gated ion channel. Proceedings of the National Academy of Sciences 108: 12149–12154. National Acad Sciences.

Hu H, Nemecz Á, Van Renterghem C, Fourati Z, Sauguet L, Corringer PJ, Delarue M. 2018. Crystal structures of a pentameric ion channel gated by alkaline pH show a widely open pore and identify a cavity for modulation. Proceedings of the National Academy of Sciences 115. National Acad Sciences.

Kruse AC, Ring AM, Manglik A, Hu J, Hu K, Eitel K, Hübner H, Pardon E, Valant C, Sexton PM, *et al.* 2013. Activation and allosteric modulation of a muscarinic acetylcholine receptor. Nature 504: 101–106. Nature Publishing Group.

Lin-Moshier Y, Marchant JS. 2013. The *Xenopus* Oocyte: A Single-cell Model for Studying Ca^{2+} Signaling. Cold Spring Harbor Protocols 2013. Cold Spring Harbor Laboratory Press.

Lodish H, Berk A, Kaiser CA, Krieger M, Bretscher A, Ploegh H, Amon A, Martin KC. 2016. Molecular Cell Biology. W.H. Freeman, New York, 8th edition.

Mowry KL. 2020. Using the *Xenopus* Oocyte Toolbox. Cold Spring Harbor Protocols 2020. Cold Spring Harbor Laboratory Press.

Nelson DL, Cox MM. 2017. Lehninger PRINCIPLES of BIOCHEMISTRY. Macmillan, New York, 7th edition.

Neubig RR, Spedding M, Kenakin T, Christopoulos A. 2003. International Union of Pharmacology Committee on Receptor Nomenclature and Drug Classification. xxxviii. Update on terms and symbols in quantitative pharmacology. Pharmacological reviews 55: 597–606. ASPET.

Pettersen EF, Goddard TD, Huang CC, Couch GS, Greenblatt DM, Meng EC, Ferrin TE. 2004. UCSF Chimera—a visualization system for exploratory research and analysis. Journal of computational chemistry 25: 1605–1612. Wiley Online Library.

Plested AJ. 2016. Structural mechanisms of activation and desensitization in neurotransmitter-gated ion channels. Nature structural & molecular biology 23: 494–502.

Rissman RA, Mobley WC. 2011. Implications for treatment: $GABA_A$ receptors in aging, Down syndrome and Alzheimer's disease. Journal of neurochemistry 117: 613–622. Wiley Online Library.

Sauguet L, Shahsavar A, Delarue M. 2015. Crystallographic studies of pharmacological sites in pentameric ligand-gated ion channels. Biochimica et Biophysica Acta (BBA)-General Subjects 1850: 511–523. Elsevier.

Spurny R, Ramerstorfer J, Price K, Brams M, Ernst M, Nury H, Verheij M, Legrand P, Bertrand D, Bertrand S, *et al.* 2012. Pentameric ligand-gated ion channel ELIC is activated by GABA and modulated by benzodiazepines. Proceedings of the National Academy of Sciences 109. National Acad Sciences.

Tanner C, Goldman S, Aston D, Ottman R, Ellenberg J, Mayeux R, Langston J. 2002. Smoking and Parkinson's disease in twins. Neurology 58: 581–588. AAN Enterprises.

Thompson AJ, Alqazzaz M, Ulens C, Lummis SC. 2012. The pharmacological profile of ELIC, a prokaryotic GABA-gated receptor. Neuropharmacology 63: 761–767. Elsevier.

Thompson AJ, Lester HA, Lummis SC. 2010. The structural basis of function in Cys-loop receptors. Quarterly reviews of biophysics 43: 449–499. Cambridge University Press.

Trott O, Olson AJ. 2010. AutoDock Vina: improving the speed and accuracy of docking with a new scoring function, efficient optimization, and multithreading. Journal of computational chemistry 31: 455–461. Wiley Online Library.

Turecek R, Trussell LO. 2001. Presynaptic glycine receptors enhance transmitter release at a mammalian central synapse. Nature 411: 587–590. Nature Publishing Group.

Unwin N. 2005. Refined structure of the nicotinic acetylcholine receptor at 4 Å resolution. Journal of molecular biology 346: 967–989. Elsevier.

Weng Y, Yang L, Corringer PJ, Sonner JM. 2010. Anesthetic sensitivity of the Gloeobacter violaceus proton-gated ion channel. Anesthesia and analgesia 110: 59. NIH Public Access.

Zampighi G, Kreman M, Boorer K, Loo D, Bezanilla F, Chandy G, Hall J, Wright E. 1995. A method for determining the unitary functional capacity of cloned channels and transporters expressed in *Xenopus laevis* oocytes. The Journal of membrane biology 148: 65–78. Springer.

Zimmermann I, Marabelli A, Bertozzi C, Sivilotti LG, Dutzler R. 2012. Inhibition of the prokaryotic pentameric ligand-gated ion channel ELIC by divalent cations. PLoS biology 10: e1001429. Public Library of Science San Francisco, USA.